Journal of Alloys and Compounds 486 (2009) 747–753

Contents lists available at ScienceDirect

Journal of Alloys and Compounds

journal homepage: www.elsevier.com/locate/jallcom

# Physical properties of alumina/yttria-stabilized zirconia composites with improved microstructure

R.H.L. Garcia, V. Ussui, N.B. de Lima, E.N.S. Muccillo, D.R.R. Lazar*

*Center of Materials Science and Technology, Energy and Nuclear Research Institute-IPEN, Av. Prof. Lineu Prestes, 2242, S. Paulo, 05508-000, SP, Brazil*

ARTICLE INFO

*Article history:*
Received 16 January 2009
Received in revised form 26 June 2009
Accepted 29 June 2009
Available online 16 July 2009

*Keywords:*
Ceramics
Chemical synthesis
Ionic conduction
Mechanical properties
Microstructure

ABSTRACT

Cubic stabilized zirconia is the preferred material for application as solid electrolyte in solid oxide fuel cells. However, this material has low fracture toughness, which can lead to formation of cracks during long-term operation. Moreover, increase of mechanical as well as electrical properties would be useful for cost-effectiveness of this type of device. In this context, addition of alumina to zirconia-based solid electrolyte can be an interesting option to accomplish that purpose. In this work, ceramic composites containing various amounts of alumina in a 9 mol% yttria-stabilized zirconia matrix were synthesized by the coprecipitation route using a low-silica zirconium precursor. Characterization techniques included scanning electron microscopy, X-ray diffraction, Vickers hardness and impedance spectroscopy. As a consequence of optimization of the synthesis route a homogeneous dispersion of the additive along with good densification was obtained. Although alumina addition to stabilized zirconia exerts a deleterious effect on the electrical conductivity, it improves the Vickers hardness and fracture toughness of the composite materials.



## 1. Introduction

Solid oxide fuel cells (SOFCs) are devices that generate electricity from the electrochemical reaction of oxidation of a combustible [1]. The most important characteristics of SOFCs are the highest theoretical efficiency of chemical/electrical energy conversion, low noise level, almost no emission of toxic gases and fuel flexibility. Nowadays, attention is focused in cost reduction for commercial purposes [1] and one of the main challenges is the selection of materials due to the high operation temperature (700–1000 °C).

The most studied material for use as solid electrolyte is the cubic stabilized zirconia (CSZ), due to its high ionic conductivity, chemical stability in oxidizing and reducing atmospheres, and low electronic conductivity. However, CSZ shows low fracture toughness, which can lead to crack formation thereby compromising the cell efficiency due to the combination of the reagent gases. To overcome this problem, alumina may be added to CSZ matrix enhancing the hardness, bending strength and fracture toughness of the ceramic [2–4]. Several publications in this subject reveal that the experimental results are still a controversial issue [5–8], although many recent reports have demonstrated the advantageous properties of zirconia–alumina composite solid electrolytes [9–12]. Therefore, additional studies are necessary to correlate the electrical and mechanical properties with the amount of alumina in low-silica zirconia solid electrolyte. Moreover, there is a consensus in the literature that the synthesis route of ceramic powders plays a key role on the definition of the microstructure, and consequently, on the mechanical and the electrical properties.

Among various chemical methods of ceramic powder synthesis, the coprecipitation route produces ceramic powders with excellent physical and chemical characteristics, by a simple procedure with inexpensive equipments [13]. This method consists in the preparation of a salt solution of the metallic precursors with a defined stoichiometry, and precipitation of metallic ions by a reaction with a precipitant solution. In general, the reagents are mixed together in an atomic scale ensuring high homogeneity, high purity and well defined stoichiometry [13–15]. Optimization of calcination and sintering conditions of the synthesized powders is of prime importance for the attainment of a homogeneous ceramic microstructure. Low calcination temperatures promote the formation of highly reactive powders, but a high temperature is often necessary for oxide formation and to eliminate organic residues [16].

Zirconia-based ceramics can be stabilized in tetragonal, cubic or monoclinic phases [17] depending on dopant concentration and on the temperature of thermal treatments. Alumina can be found as α-phase, which is stable at room temperature, or many other metastable forms as registered in the literature [18]. The variety of alumina phases is a function of the employed synthesis route, of the thermal decomposition of aluminum salts and hydroxides, and of the presence of impurity ions [18,19]. The crystallization processes of zirconia and alumina occur at distinct temperatures, and are mutually inhibited when they are mixed together [14,20]. Most

* Corresponding author. Tel.: +55 11 3133 9224; fax: +55 11 3133 9276.
*E-mail address:* drlazar@ipen.br (D.R.R. Lazar).

0925-8388/$ – see front matter © 2009 Elsevier B.V. All rights reserved.
doi:10.1016/j.jallcom.2009.06.204

of previous works were performed on ceramic composites prepared by the addition of alumina to yttria-stabilized zirconia powders. The final microstructure of the composites, in this case, is dependent on the degree of homogeneity acquired with dispersion of the second phase material.

The aim of this work is to evaluate the influence of alumina on the ionic conductivity, hardness and fracture toughness of 9 mol% yttria-stabilized zirconia (9YSZ) synthesized by the coprecipitation route using a low-silica zirconium precursor. Zirconia–alumina composites were prepared varying the concentration of alumina from 1 to 40 wt.%. 8YSZ (8 mol% yttria-stabilized zirconia) ceramic compacts were also prepared from a commercial powder for comparison purposes. The synthesis procedures were optimized to obtain a homogeneous dispersion of the additive in the zirconia matrix.

## 2. Experimental procedures

### 2.1. Sample preparation

Zirconium hydroxide (99.5%, IPEN, Brazil), yttrium oxide (99.9%, Aldrich) and aluminum chloride (99%, Synth) were used as starting materials. Zirconium precursor material was obtained by decomposition of zircon by alkaline fusion followed by purification process by precipitation of basic zirconium sulfate. Addition of ammonium hydroxide to zirconium basic sulfate replaced sulfate ions by hydroxyl groups providing zirconium hydroxide with relatively low-silica content (<300 ppm). Stock solutions of zirconium oxychloride and yttrium chloride were prepared by dissolution of the respective starting materials in HCl solution. All other reagents used during synthesis were of analytical grade. The preparation of 9 mol% yttria-stabilized zirconia–$x$% alumina with $1 \leq x \leq 40$ wt.% was carried out by the simultaneous precipitation of cations followed by azeotropic distillation.

To determine the volume of ammonium hydroxide necessary for maximum efficiency, a titration test was performed for the three chloride solutions with a 3 M $NH_4OH$ solution. From this result, the coprecipitation experiments were set up for producing 35 g of mixed oxides per batch.

The hydroxide coprecipitation was performed with slow addition of mixed chloride solution to the precipitant solution under vigorous stirring. The pH of the mother liquor was maintained higher than 10. Subsequently, the suspension was kept under stirring for 15 min to ensure good homogeneity. The precipitate was washed with water several times until the filtrated indicated the absence of $Cl^-$, and treated with ethanol and $n$-butanol to remove the bulk water. Dehydration of the precipitate was completed by azeotropic distillation. Finally, the precipitate was dried at 80 °C for 24 h, deagglomerated in an agate mortar, calcined and milled with zirconia balls for 16 h in ethanol. The calcination of the precipitates was performed in air at 600 or 800 °C for 1 h. After milling, cylindrical pellets were prepared by uniaxial pressing at 100 MPa followed by sintering at 1500 and 1620 °C for 1 h. Commercial 8YSZ powder (Tosoh, Japan) was pressed and sintered using the same conditions for comparison purposes. The produced powders and sintered compacts are identified as $x$ACZ, where "$x$" denotes the wt.% of alumina in a 9 mol% yttria-stabilized zirconia matrix, and 8YSZ, for the sample prepared with commercial powder.

### 2.2. Characterization methods

Powders were characterized by determination of specific surface area by gas adsorption technique (Micromeritics ASAP 2000) using the BET method; measurements of granulometric distribution of agglomerates by laser diffraction (Beckman-Coulter LS 13 320 with tornado DPS module); observation of particle and agglomerate morphologies by scanning electron microscopy, SEM (Philips XL30) and transmission electron microscopy, TEM (JEOL 200C), and crystalline phase identification by X-ray diffraction, XRD (Rigaku Multiflex) using Cu Kα radiation.

Characterization of sintered samples included density measurements based on Archimedes principle using distilled water. Observation of polished surfaces by scanning electron microscopy was performed on previously thermally etched samples. The mean grain size of these samples was determined using the Image-Pro Plus 4.1.0.0 software. X-ray diffraction measurements were carried out for phase analysis, and Rietveld refinement was used for phase quantification. In this case, XRD patterns were recorded with 8 s of counting time per 0.02° step size. Hardness and fracture toughness were obtained by Vickers indentation tests (Buehler VMT-7 and MM-3) [21]. The applied load was 19 N for most of the samples except for 40ACZ (49 N). Vickers hardness was calculated by:

$$H_v = \frac{\alpha P}{d^2}$$

where $P$ is the applied load (N), $d$ is the average diagonal length (m), and $\alpha$ is the angle between the opposite faces of the indenter (136°). The fracture toughness ($K_{1c}$) was determined by the following equation for radial-median cracks [22]:

$$K_{1c} = 0.0154 \left(\frac{E}{H_v}\right)^{1/2} \left[\frac{P}{(c+l)^{3/2}}\right]$$

where $K_{1c}$ is given in MPa m$^{1/2}$, $E$ is the elastic modulus (GPa), $c$ is the semidiagonal impression length (m) and $l$ is the crack length (m).

Resistance measurements on sintered samples were done by electrochemical impedance spectroscopy (HP 4192A). These measurements were carried in air at temperatures between 200 and 550 °C, and 5 Hz to 13 MHz frequency range. Sintered samples were previously coated with silver paste (Cerdec PO2008) and fired at 400 °C for this analysis. The electrical conductivity, $\sigma$, of samples was calculated by:

$$\sigma T = \sigma_0 \exp\left(-\frac{E}{kT}\right)$$

where $\sigma_0$, $E$, $k$ and $T$ are the pre-exponential factor, the apparent activation energy, the Boltzmann constant and the absolute temperature, respectively.

## 3. Results and discussion

### 3.1. Powder characterization

Fig. 1a and b shows SEM micrographs of the calcined (800 °C/1 h) powders with different alumina contents. All powder materials consist of agglomerates of submicron size. The degree of agglomeration is similar for all prepared compositions independent on alumina content. Fig. 1c exhibits the SEM micrograph of the commercial 8YSZ powder consisting of granules of varying sizes. This material is also prepared by coprecipitation followed by a step of spray drying after milling. The agglomerated powders synthesized by coprecipitation in this work are constituted by nanosized particles as shown in the bright-field TEM micrograph of Fig. 1d.

Fig. 2 shows the XRD patterns of composite powders and commercial material. These diffraction patterns exhibit the reflections of the cubic fluorite-type phase (indicated in the bottom of the figure). Increase of the alumina content produces a gradual decrease in the relative intensity of cubic zirconia peaks and a simultaneous broadening of the diffraction peaks, even for calcination temperatures as high as 800 °C. This result indicates that for these composite materials a higher calcination temperature is necessary to attain the same crystallinity obtained for yttria-stabilized zirconia prepared by the same technique [16].

Addition of alumina to yttria-stabilized zirconia also produces a significant increase of the specific surface area from ~10 to 150 m$^2$ g$^{-1}$ for samples containing 0 to 40 wt.% $Al_2O_3$ (Fig. 3a). Considering that during the crystallization process, the specific surface area is reduced due to elimination of micropores, this result also suggests that the addition of alumina inhibits the composite crystallization in agreement with XRD patterns.

Another effect resulting from alumina addition to 9YSZ is the reduction of the agglomerate size shown by granulometric analysis (Fig. 3b) from about 4 (1ACZ) to 2.5 (20ACZ) μm. The commercial powder 8YSZ is constituted by large agglomerates with medium size of ~7 μm.

### 3.2. Density and microstructure of sintered composites

The study of sintered materials was carried out with powders calcined at 800 °C/1 h. The evolution of the relative density of sintered composite samples with alumina content is shown in Fig. 4. Samples containing nominal 1, 3 and 5 wt.% $Al_2O_3$ were sintered at 1500 and 1620 °C to verify the effect of the dwell temperature on densification of low alumina-zirconia composites. All samples reached relative densities higher than 95% of theoretical density (TD). 1ACZ and 3ACZ ceramics attained a relative density higher than 98% at 1500 °C. In contrast, the sample 5ACZ showed higher density when sintered at 1620 °C. Therefore, samples 1ACZ and

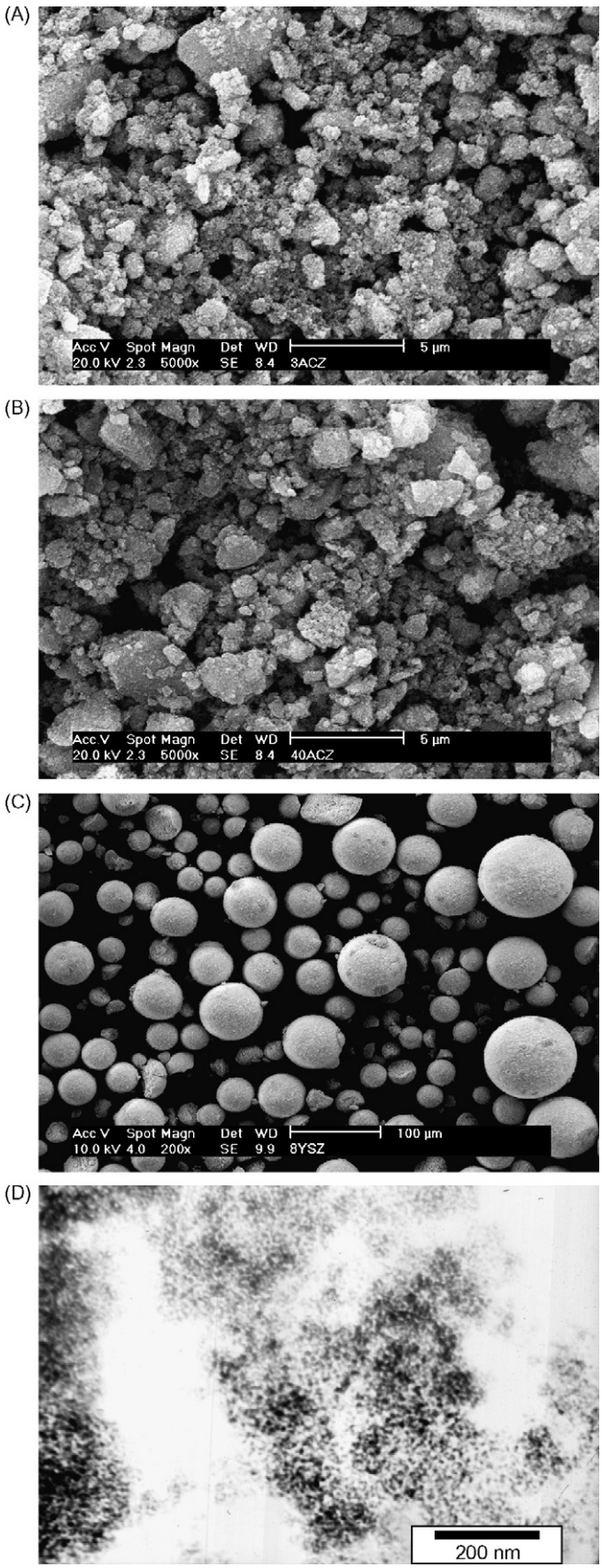


**Fig. 1.** SEM micrographs (a, b and c) obtained for zirconia–alumina powders: (a, b) synthesized in this work (respectively, 3ACZ and 40ACZ), (c) commercial 8YSZ and (d) bright-field TEM micrograph of 20ACZ sample.

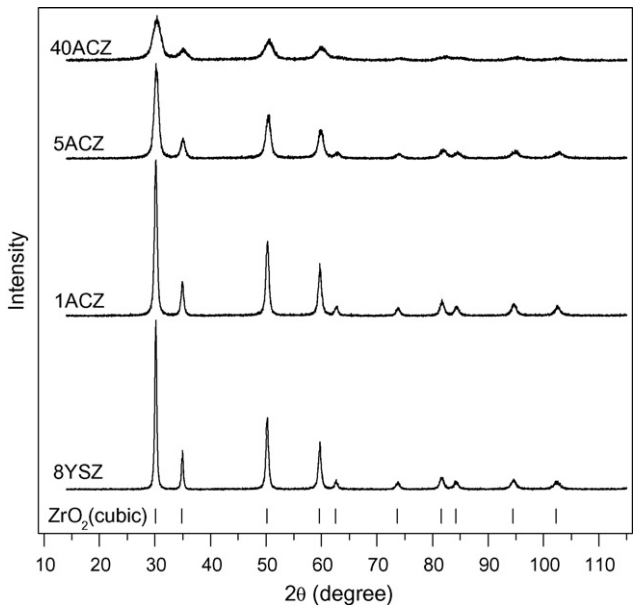


**Fig. 2.** XRD patterns of zirconia–alumina powders, containing 0, 1, 5 and 40 wt.% alumina.

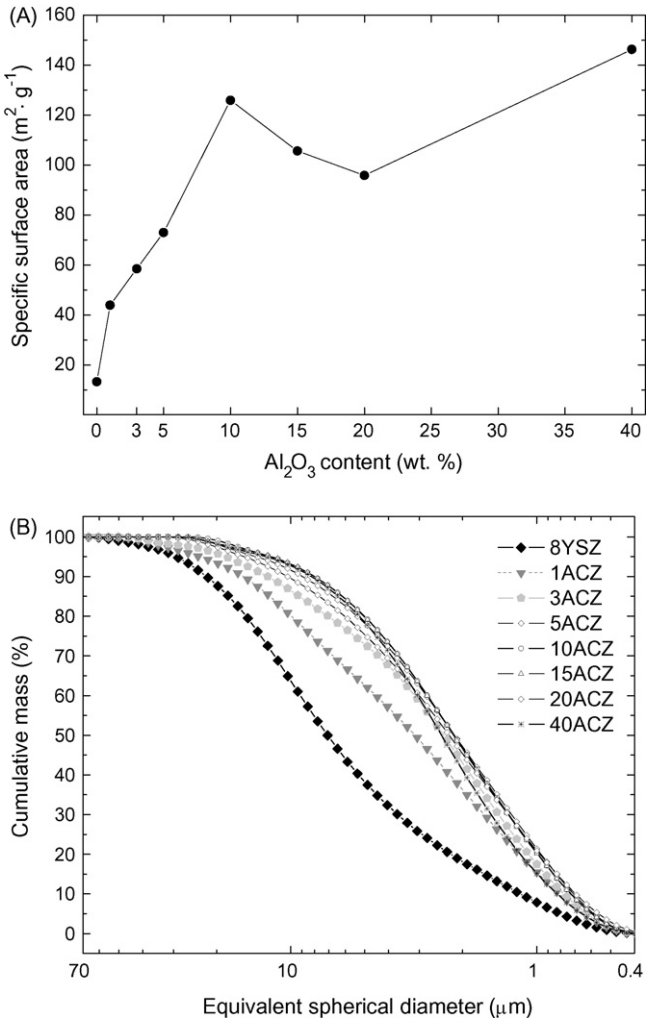


**Fig. 3.** (a) Specific surface area and (b) granulometric distribution of zirconia–alumina powders containing 0–40 wt.% alumina.

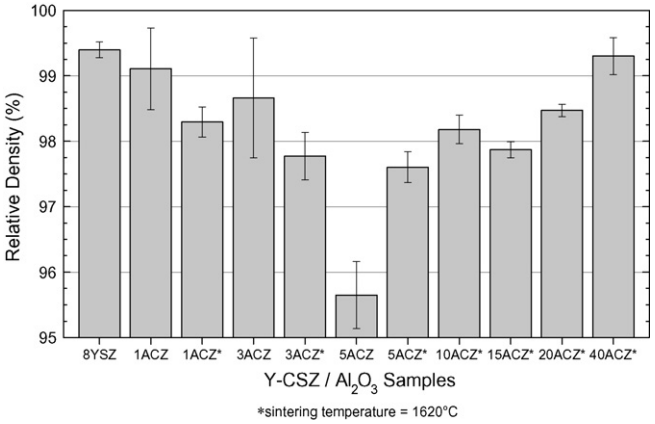


**Fig. 4.** Relative density values of zirconia–alumina composites sintered at 1500 and 1620 °C and containing different amounts of alumina.

**Table 1**
Values of medium grain sizes of zirconia–alumina composites containing 0–40 wt.% alumina.

| Sample | Medium grain size (μm) | |
|---|---|---|
| | Y-CSZ | $\alpha$-$Al_2O_3$ |
| 8YSZ | 7.5 ± 3.0 | – |
| 1ACZ | 7.1 ± 2.6 | 0.74 ± 0.28 |
| 3ACZ | 4.2 ± 1.4 | 0.52 ± 0.15 |
| 5ACZ | 5.6 ± 3.0 | 0.71 ± 0.25 |
| 10ACZ | 3.1 ± 1.4 | 0.87 ± 0.33 |
| 15ACZ | 2.5 ± 0.95 | 0.73 ± 0.40 |
| 20ACZ | 2.1 ± 080 | 0.97 ± 050 |
| 40ACZ | 1.2 ± 0.44 | 1.00 ± 0.37 |

3ACZ sintered at 1500 °C and 5ACZ sintered at 1620 °C were selected for subsequent characterization.

Fig. 5 shows SEM micrographs of polished and thermally etched surfaces of alumina-zirconia composites. The relevant aspects of microstructure in these micrographs are relatively low porosity and

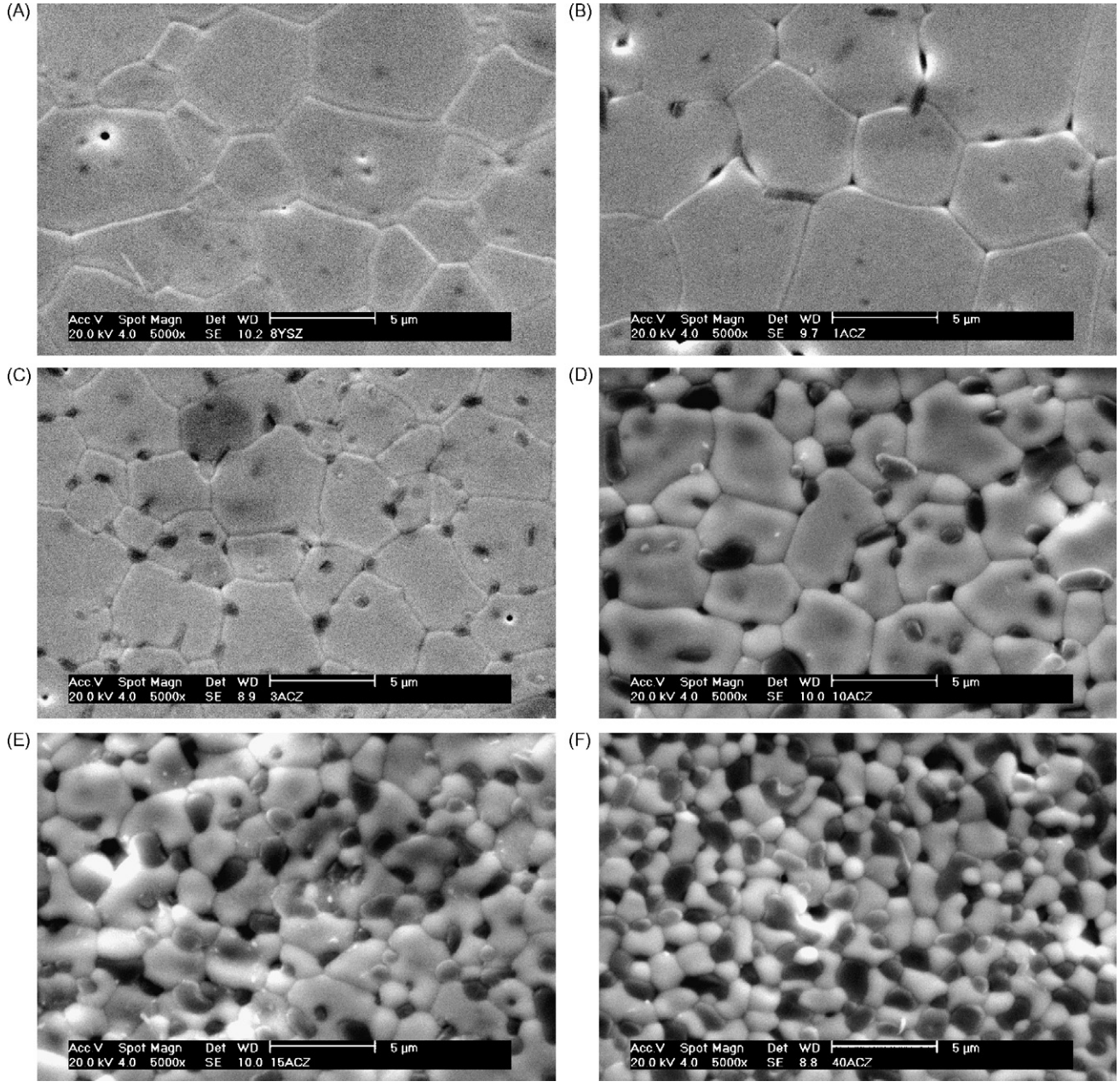


**Fig. 5.** SEM micrographs of polished surfaces of composites: (a) 8YSZ, (b) 1ACZ, (c) 3ACZ, (d) 10ACZ, (e) 15ACZ and (f) 40ACZ.

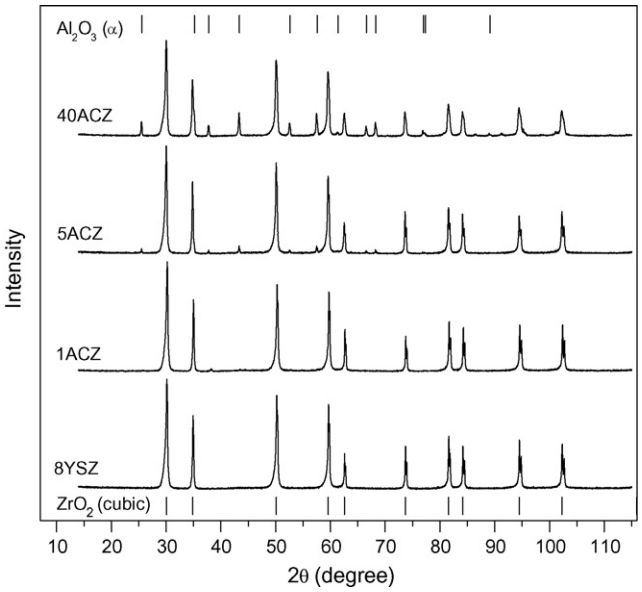


**Fig. 6.** XRD patterns of zirconia–alumina composites containing 0, 1, 5 and 40 wt.% alumina.

good homogeneity. Alumina grains are randomly dispersed in the matrix. As can be seen in these micrographs, the size of zirconia grains reduces with increasing alumina addition. Table 1 shows mean grain size values of studied composites determined in a large number of grains. There is a remarkable reduction of the zirconia matrix mean grain size with alumina addition reaching ~1 μm for 40 wt.% alumina.

XRD patterns of sintered composites (Fig. 6) show the evolution of α-alumina diffraction peaks (indicated in the top of the Fig.) and the consequently decrease of cubic zirconia reflections. Moreover, it is confirmed the crystallinity of the zirconia and alumina phases, whose contents were calculated using the Rietveld method. The obtained results are 0.5, 3.0, 5.8, 11.5, 18.1, 20.5 and 39.0 wt.% of α-alumina in 9YSZ matrix for samples 1ACZ, 3ACZ, 5ACZ, 10ACZ, 15ACZ, 20ACZ and 40ACZ, respectively.

### 3.3. Electrical and mechanical properties of composites

Impedance spectroscopy diagrams of samples 8YSZ, 1ACZ and 5ACZ, recorded at 350 °C are plotted in Fig. 7. All diagrams consist of two well-resolved semicircles in the frequency and temperature ranges of measurements. The impedance diagrams were normalized for sample dimensions, and no corrections were made for porosity, once only samples with relative densities higher than 98% were analyzed. Alumina addition to 9YSZ changes both the grain (high frequency) and the grain boundary (low frequency) resistivity even at low additive contents. However, due to the well-known low solubility of alumina in zirconia (less than 1 wt.%), its effect on grain conductivity is of minor importance. A small decrease in the grain conductivity of 8YSZ with increasing alumina additions has

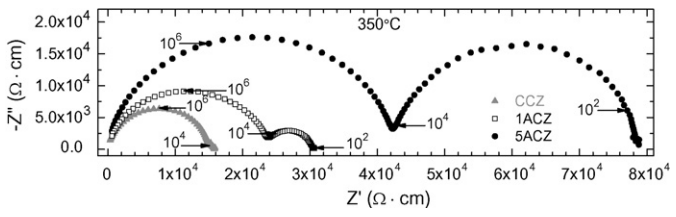


**Fig. 7.** Impedance spectroscopy diagrams of zirconia–alumina composites. Temperature of measurement = 350 °C.

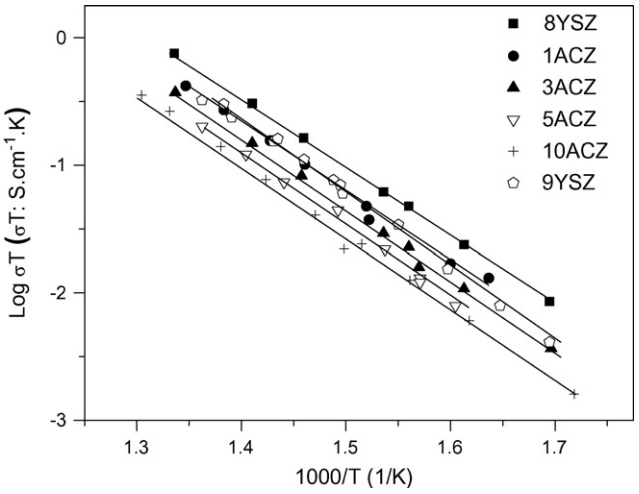


**Fig. 8.** Arrhenius plots of the total ionic conductivity of 8YSZ, 9YSZ and zirconia–alumina composites containing 0, 1, 3, 5 and 10 wt.% alumina.

been previously reported [12]. Then, the benefit of alumina to the ionic conductivity of yttria-stabilized zirconia was proposed to be related to impurity phases usually present at the grain boundaries [12].

Fig. 8 shows Arrhenius plots of the total ionic conductivity of sintered composites containing up to 10 wt.% alumina. All composites exhibit a thermally activated behavior with lower ionic conductivity magnitude than that of 8YSZ. In this figure the conductivity of a 9YSZ sample prepared by the same method under similar experimental conditions was introduced also for comparison purposes [23].

The commercial 8YSZ ceramic has the highest ionic conductivity among the studied materials. The ionic conductivity of 9YSZ sample is quite similar to that of 1ACZ composite material. The actual content of alumina (0.5 wt.%) in 1ACZ samples is near the solubility limit at the sintering temperature. In this case, its effect is mostly on the grain conductivity, which seems to be negligible according to results in Fig. 8. The total ionic conductivity of composite materials decreases with increasing of the alumina content. Then, it may be concluded that alumina addition has a deleterious effect on low-silica yttria-stabilized zirconia. Apparent activation energy values for the studied materials shown in Table 2 are similar within experimental errors.

Concerning the mechanical properties of the synthesized ceramic materials, it was obtained a linear increase of Vickers hard-

**Table 2**
Apparent activation energy values for the total ionic conductivity and fracture toughness of studied samples and from literature.

| Sample | Activation energy (eV) | Fracture toughness (MPa m$^{1/2}$) | Reference |
|---|---|---|---|
| 8YSZ | 1.08 ± 0.05 | 1.69 ± 0.14 | This work |
| 8YSZ | 0.82 | 2.05 | [5] |
| 8YSZ | 1.02 | 2.00 | [8] |
| 1ACZ | 1.07 ± 0.05 | 1.68 ± 0.28 | This work |
| 3ACZ | 1.12 ± 0.05 | 2.16 ± 0.14 | This work |
| 5ACZ | 1.15 ± 0.05 | 2.41 ± 0.44 | This work |
| 10ACZ | 1.13 ± 0.05 | 2.63 ± 0.13 | This work |
| 15ACZ | – | 3.47 ± 0.54 | This work |
| 20ACZ | – | 3.42 ± 0.59 | This work |
| 8YSZ + 10 wt.% alumina | 1.13 | 2.40 | [8,24] |
| 8YSZ + 15 wt.% alumina | – | 2.20 | [2] |
| | – | 2.70 | [5] |
| 8YSZ + 20 wt.% alumina | – | 2.43 | [2] |
| | – | 2.90 | [5] |
| 8YSZ + 25 wt.% alumina | 0.78 | 3.20 | [5] |
| 9YSZ | 1.16 ± 0.05 | – | [23] |

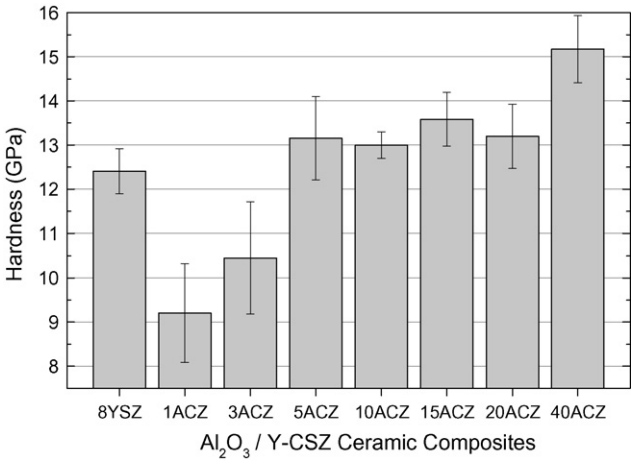


**Fig. 9.** Vickers hardness of zirconia–alumina composites containing up to 40 wt.% alumina.

ness with the amount of alumina in the composite (Fig. 9). Samples prepared with commercial powder (8YSZ) exhibit hardness comparable to those of samples 3ACZ and 5ACZ. This fact can be explained by the better density attained and the lower amount of yttria in the commercial material (8 mol% instead of 9 mol%). This difference in the yttria content could lead to the formation of a small amount of tetragonal phase, thereby improving its mechanical properties. The increase of hardness with alumina addition can be explained by three factors [2,3,8]: (1) growth restriction of zirconia grains on sintering; (2) crack deflection mechanism and (3) formation of internal stresses due to different thermal expansion coefficients and to distinct elastic modulus of the constituents.

An optical image of 30ACZ sample after indentation and brief polishing is shown in Fig. 10. The cracks emanating from the four vertices demonstrate a large depth below the surface which is an evidence of radial-median crack morphology [22]. Similar observation was found in thin films [25].

Fig. 11 shows scanning electron microscopy micrographs of 20ACZ and 30ACZ samples after indentation and thermal etching and the results of fracture toughness of the composites. A homogeneous distribution of alumina grains in the composite may be seen. The fracture crack is almost intergranular and tends to follow the grain boundary in a ziz-zag manner (crack deflection). This behavior results in greater fracture energy leading to increased fracture

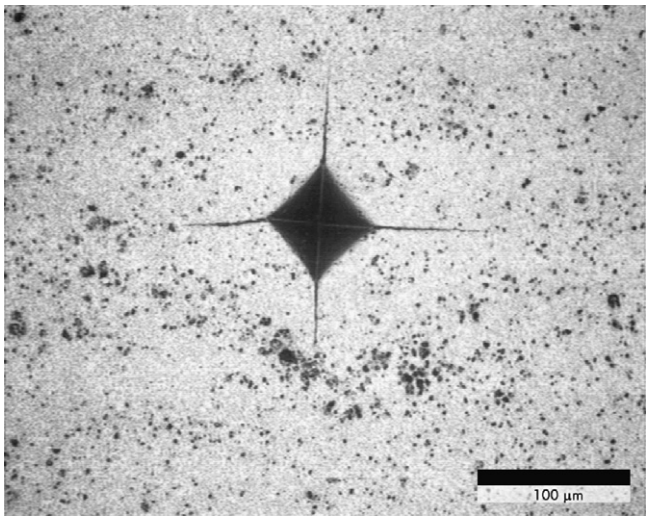


**Fig. 10.** Optical micrograph of 30ACZ sample after indentation and brief polishing.

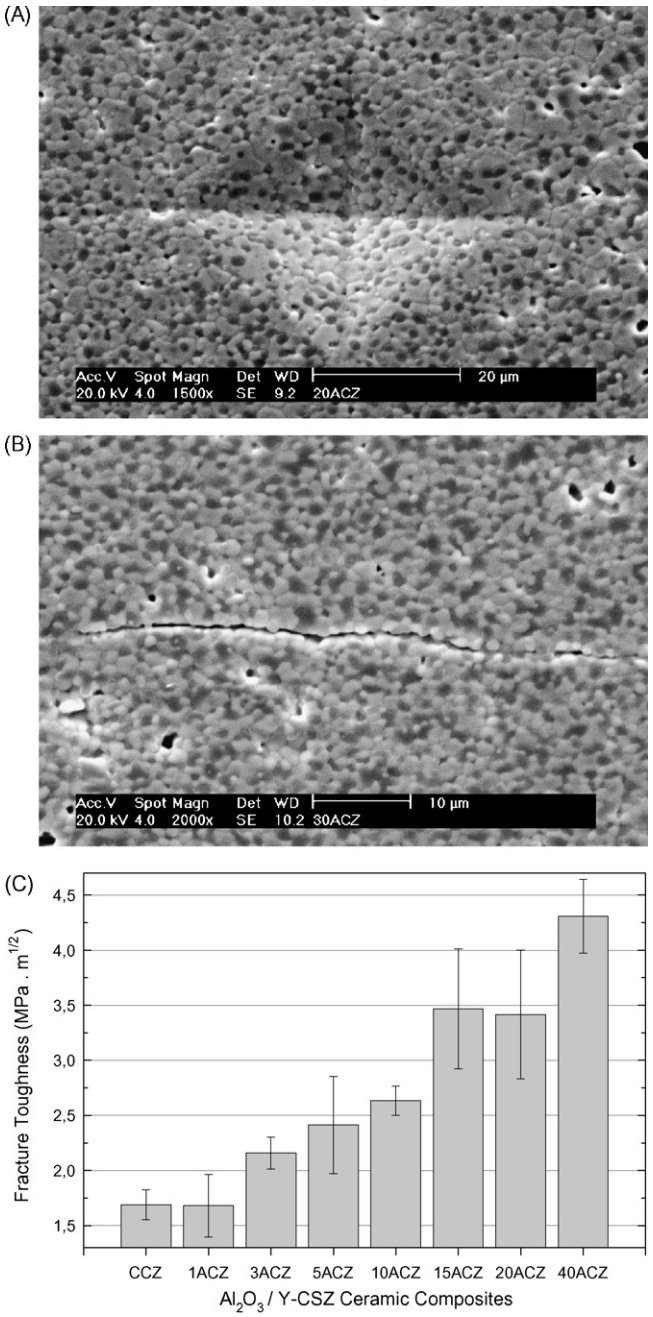


**Fig. 11.** SEM micrographs of 20ACZ and 30ACZ samples after indentation and thermal etching (a and b) and fracture toughness of zirconia–alumina composites containing up to 40 wt.% alumina (c).

toughness for samples with higher content of alumina. A more general discussion on crack formation during indentation may be found in [26]. Values of fracture toughness for selected alumina contents are shown in Table 2 along with those of previous investigations. It is worth to note the relatively high values obtained in this work for the same alumina content. This fact may be attributed to the good dispersion of alumina grains in the zirconia matrix attained by the employed method of synthesis.

## 4. Summary and conclusions

The coprecipitation technique demonstrated to be an efficient route to obtain zirconia–alumina ceramic composites with relatively high homogeneity. Alumina addition to 9YSZ matrix increases

the specific surface area and inhibits the crystallization of powders. Independent on the alumina content, all composites exhibited primary particles in the nanosize range and similar state of agglomeration. Additionally, all the ceramic composites attained high density, homogeneous microstructure and good crystallinity. At the same sintering conditions, the increase of alumina content delays the crystallization and densification of the composites. Alumina addition to 9YSZ matrix has a deleterious effect on the total ionic conductivity, whenever the precursor material has low-silica content. The addition of alumina to 9YSZ enhanced the Vickers hardness and the fracture toughness of the composite providing fracture toughness values even higher than pure CSZ or alumina.

## Acknowledgements

The authors would like to thank FAPESP and CAPES for financial support, LAMI (Laboratório Associado Micronal & IPT) for granulometric measurements, and J.D. Andrade, S.M. Cunha, R.R. de Oliveira, C.V. de Moraes and N.A.M. Ferreira for technical assistance.

## References

[1] N.Q. Mihn, Solid State Ionics 174 (2004) 271–277.
[2] S.R. Choi, N.P. Bansal, Ceram. Int. 31 (2005) 39–46.
[3] N.H. Kwon, G.H. Kim, H.S. Song, H.L. Lee, Mater. Sci. Eng. A 299 (2001) 185–194.
[4] M. Szutkowska, J. Mater. Process. Technol. 153–154 (2004) 868–874.
[5] K. Oe, K. Kikkawa, A. Kishimoto, Y. Nakamura, H. Yanagida, Solid State Ionics 91 (1996) 131–136.
[6] X. Guo, R. Yuan, J. Mater. Sci. 30 (1995) 923–931.
[7] X. Guo, J. Am. Ceram. Soc. 86 (2003) 1867–1873.
[8] L.M. Navarro, P. Recio, J.R. Jurado, P. Duran, J. Mater. Sci. 30 (1995) 1949–1960.
[9] J.S. Thokchom, H. Xiao, M. Rottmayer, T.L. Reitz, B. Kumar, J. Power Sources 178 (2008) 26–33.
[10] A. Peters, C. Korte, D. Hesse, N. Zakharov, J. Janek, Solid State Ionics 178 (2007) 67–76.
[11] R. Knibbe, J. Drennan, A. Dicks, J. Love, J. Power Sources 179 (2008) 511–519.
[12] D. Lyebye, Y.-L. Liu, J. Eur. Ceram. Soc. 26 (2006) 599–604.
[13] D.W. Johnson Jr., Bull. Am. Ceram. Soc. 60 (1981) 221–224.
[14] J.L. Shi, B.S. Li, M.L. Ruan, T.S. Yen, J. Eur. Ceram. Soc. 15 (1995) 959–965.
[15] R.H.L. Garcia, V. Ussui, N.B. Lima, D.R.R. Lazar, Mater. Sci. Forum. 530–531 (2006) 677–682.
[16] D.R.R. Lazar, C.A.B. Menezes, V. Ussui, A.H.A. Bressiani, J.O.A. Paschoal, J. Eur. Ceram. Soc. 22 (2002) 2813–2820.
[17] D.J. Green, R.H.J. Hannink, M.V. Swain, Transformation Toughening of Ceramics, CRC, Florida, 1989.
[18] L.D. Hart, Alumina Chemicals: Science and Technology Handbook, The American Ceramic Society, Ohio, 1990.
[19] M. Ozawa, Y. Nishio, J. Alloys Compd. 374 (2004) 397–400.
[20] S. Bhattacharyya, S.K. Pratihar, R.K. Sinha, R.C. Behera, R.I. Ganguly, Mater. Lett. 53 (2002) 425–431.
[21] A. Iost, R. Bigot, J. Mater. Sci. 31 (1996) 3573–3577.
[22] G.R. Antis, P. Chantikul, B.R. Lawn, D.B. Marshall, J. Am. Ceram. Soc. 64 (1981) 533–538.
[23] D.R.R. Lazar, V. Ussui, E.N.S. Muccillo, A.H.A. Bressiani, J.O.A. Paschoal, Mater. Sci. Forum. 498 (2005) 305–310.
[24] S. Tekeli, Compos. Sci. Technol. 65 (2005) 967–972.
[25] X. Li, B. Bhushan, Thin Solid Films 355–356 (1999) 330–336.
[26] X. Li, B. Bhushan, Thin Solid Films 398–399 (2001) 313–319.